A Technique for Determining the Carrier Phase Differences between Independent GPS Receivers during Scintillation

Shan Mohiuddin, Todd E. Humphreys, and Mark L. Psiaki
Cornell University

BIOGRAPHY

Shan Mohiuddin is a graduate student in Mechanical and Aerospace Engineering. He received a B.S. in Aerospace Engineering from Virginia Tech in 2003 and has worked in the Flight Dynamics Analysis Branch at NASA/Goddard Space Flight Center. His research focuses on navigation algorithms for spacecraft, estimation theory, and GNSS receiver technology.

Todd E. Humphreys is a post-doctoral researcher in Mechanical and Aerospace Engineering. He received a B.S. and M.S. in Electrical and Computer Engineering from Utah State University and a Ph.D. in Mechanical and Aerospace Engineering from Cornell University. His research interests are in estimation and filtering, spacecraft attitude determination, GNSS technology, and GNSS-based study of the ionosphere and neutral atmosphere.

Mark L. Psiaki is a Professor of Mechanical and Aerospace Engineering. He received a B.A. in Physics and M.A. and Ph.D. degrees in Mechanical and Aerospace Engineering from Princeton University. His research interests are in the areas of estimation and filtering, spacecraft attitude and orbit determination, and GNSS technology and application.

ABSTRACT

A method for recovering the carrier phase differences between pairs of independent GPS receivers has been developed and demonstrated in truth-model simulations. This effort is in support of a project that intends to image the disturbed ionosphere with diffraction tomography techniques using GPS measurements from large arrays of receivers. Carrier phase differential GPS techniques, common in surveying and relative navigation, are employed to determine the phase relationships between the receivers in the imaging array. Strategies for estimating the absolute carrier phase disturbances at each receiver are discussed. Simulation results demonstrate that the system can rapidly detect the onset of scintillation, identify one non-scintillating reference signal, and recover the carrier phase differences accurate to 0.1 cycles.

INTRODUCTION

GPS radio waves experience several changes as they pass through the ionosphere. A quiet ionosphere introduces the well-known code delay and phase advance effects. The left half of Fig. 1 depicts the scenario where a GPS signal passes through a quiet portion of the ionosphere to a receiver situated on the ground. If the electron density profile changes slowly across this portion of the ionosphere, the signal may be assumed to have a single ionospheric pierce point. Thus the signal is altered only by the number of free electrons encountered along its direct path from the satellite to the receiver. This quantity, defined as the total number of electrons in a 1-m^2 cross section column that is oriented along the signal's path, is called the Total Electron Content (TEC). Such a slowly varying electron density profile is represented in the left panel of Fig. 2. In this quiet ionosphere model, which will be referred to in this paper as the bulk-quiescent ionosphere model, the received signal is characterized by an amplitude that is independent of $TEC(x)$ and a phase that is a function of the electron density at the signal's pierce point $TEC(x_1)$.[1]

When electron density irregularities are present, the effect on the signals is more complicated. This situation is depicted in the right half of Fig. 1 where the signal is re-

[1] The horizontal dimension x is aligned perpendicular to the local magnetic field at the ionospheric pierce point. This orientation takes advantage of the fact that ionospheric irregularities, when present, tend to align along the local magnetic field lines. Hence, variations in TEC exist primarily along only one horizontal direction.

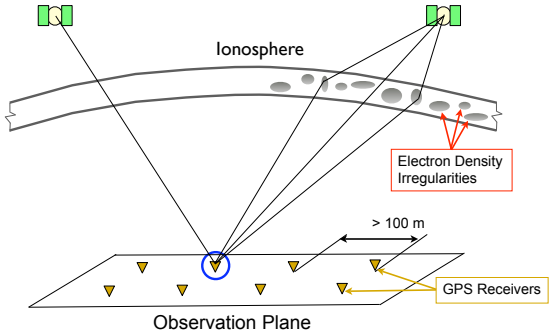

Figure 1. The undisturbed and disturbed ionosphere and the scintillation imaging array.

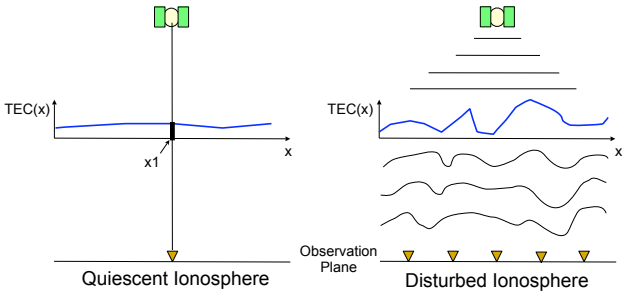

Figure 2. The bulk-quiescent ionosphere mode (left) and the wave propagation model (right).

fracted and diffracted by the irregularities. The signal not only experiences code delay and phase advance due to the free electrons along the propagation path but also experiences constructive and destructive interference as the disturbed wavefront propagates down to the receiver. In this case, the bulk-quiescent ionosphere model is inadequate to describe the signal disturbances; a more complex model, based on the physics of wave propagation through irregular media, is required. Such a model is depicted in the right panel of Fig. 2, where the transmitted wavefront encounters a TEC profile that varies significantly along the x direction. The uneven lines below the modeled ionosphere represent phase variations in the propagating wavefront. The received signal's amplitude and phase are now dependent on the electron density profile along the x axis. The signal at the observation plane exhibits deep power fades and carrier phase disturbances referred to respectively as amplitude and phase scintillation [1]. As an illustraton of the effect of scintillation, Fig. 3 shows a time history of the received carrier-to-noise ratio and carrier phase disturbances for a scintillating signal.

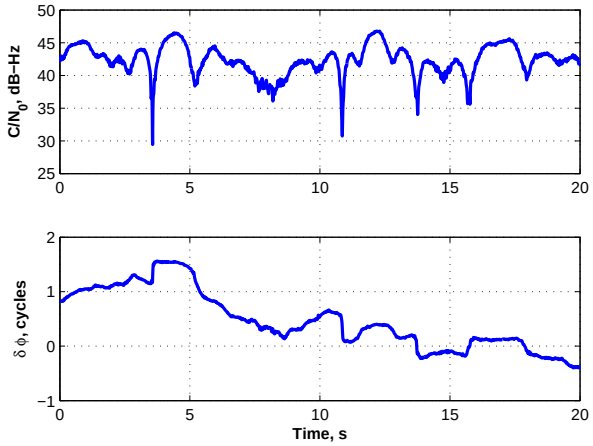

Figure 3. A time history of the received carrier-to-noise ratio (top) and the scintillation-induced phase disturbances (bottom).

The study of ionospheric disturbances and their effects on GPS signals is of both practical and scientific interest. For GPS users, especially those who use carrier phase techniques for precise relative positioning, the disturbances caused by scintillation pose a significant problem. During quiet periods, ionospheric effects may be removed using models, dual-frequency measurements (if available), or differencing techniques. The latter approach, often used in surveying and relative navigation applications, relies on the single pierce point and smooth TEC profile assumptions to cancel out the effects of the ionosphere over short baselines. These assumptions break down if the GPS signals are scintillating. In this case, precise positioning may be impossible.

For ionospheric scientists, the altered GPS signals offer insight into the structure and dynamics of the disturbed ionosphere. A project is underway at Cornell University that intends to use arrays of tens, hundreds, or even thousands of inexpensive GPS receivers spread out over tens of kilometers to image the disturbed ionosphere through diffraction tomography. This project will used techniques similar to those discussed in Ref. [2] to reconstruct TEC profiles based on terrestrial GPS measurements and on wave propagation models. Figure 1 shows a schematic of small segment of the envisioned scintillation imaging array.

Signal amplitude is relatively easy to measure with

an array of calibrated receivers, but it only represents part of the received signal. The other part, the signal's phase, is more difficult to measure because a proper measurement would require the array to be phase-synchronized. The envisioned array, however, is too large for the receivers to be connected to a common phase reference. Thus, each receiver must use its own independent clock to make its phase measurements. This introduces phase biases into the measurements because the individual clock errors are inseparable from the phase measurements.

The question becomes this: What phase information can be gained from a non-phase-synchronized array? One answer, rather oddly, comes from the fields of surveying and relative navigation for which these signal disturbances represent a nuisance. The answer is that phase differences between pairs of independent receivers may be recovered using carrier phase differential GPS (CDGPS) techniques—the techniques that surveyors and navigators use to produce precise relative position estimates. Under certain circumstances, these phase relationships may be used as science data in diffraction tomography. This paper presents a method that provides this previously unexploited carrier phase data and describes the circumstances under which these data may be exploited to image the ionosphere. Until now, the proposed imaging techniques only considered amplitude data. By providing a more complete description of the disturbed wavefront at the observation plane, the proposed method will improve the quality of the diffraction tomography estimates. The paper describes a technique for recovering carrier phase differences between pairs of receivers, demonstrates the algorithm in truth-model simulations, and illustrates the circumstances in which these data may be useful in ionospheric tomography.

The remainder of this paper is divided into five major sections. The first section describes carrier phase techniques for relative navigation and how they may be used to produce phase data from a scintillation imaging array. The second section discusses how these data may contribute to the tomography effort. The third section develops the algorithm for determining the phase differences between receivers. The fourth section describes the simulations and presents the results. The fifth section offers conclusions.

RELATIVE NAVIGATION AND SCINTILLATION

Relative navigation using CDGPS is a method by which the relative position of a pair of receivers is determined using accurate but biased carrier phase measurements. Centimeter-level accuracies, or better, are possible over short baseline distances of less than 10 *km* [3]. Figure 4 depicts a relative navigation scenario in which the relative position vector $\underline{x}$ between receivers A and B is estimated using carrier phase

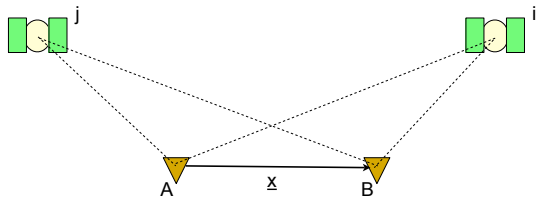

Figure 4. The relative navigation scenario.

measurements from pairs of GPS satellites. Only one pair, i and j, is included in the figure. Following the model developed in Ref. [4], the carrier phase measurement at receiver A from GPS satellite j may be written as follows:

$$\lambda\phi_A^j = \rho_A^j + c(\delta t_A - \delta t^j) + \lambda(\gamma_{0_A} - \psi_0^j) + I_A^j + T_A^j + \nu_A^j \quad (1)$$

where λ is the nominal GPS carrier wavelength, ϕ_A^j is the measured carrier phase in cycles, ρ_A^j is the line-of-sight range from satellite j to receiver A, c is the speed of light in a vacuum, δt_A is the receiver clock error for receiver A, δt^j is the satellite clock error for satellite j, γ_{0_A} is the real-valued carrier phase bias associated with receiver A, ψ_0^j is the real-valued carrier phase bias associated with satellite j, I_A^j is the bulk-quiescent ionosphere phase advance expressed as an equivalent distance, T_A^j is the troposphere delay expressed as an equivalent distance, and ν_A^j is a noise term that models thermal noise and multipath.

To eliminate terms that are common to a particular GPS satellite, measurements from the two receivers are differenced. A single-difference operator, defined as $\Delta(*)_{AB}^j = (*)_B^j - (*)_A^j$, is used in the following single-differenced measurement equation:

$$\lambda\Delta(\phi)_{AB}^j = \Delta(\rho)_{AB}^j + c(\delta t_B - \delta t_A) + \lambda(\gamma_{0_B} - \gamma_{0_A}) + \Delta(\nu)_{AB}^j \quad (2)$$

In the bulk-quiescent ionosphere model, the single differenced atmospheric terms may safely be neglected over short baselines. Those terms have been dropped from Eq. (2). The clock terms and bias terms associated with satellite j cancel out. A single-differenced receiver clock term $c(\delta t_B - \delta t_A)$ and a single-differenced bias term $\lambda(\gamma_{0_B} - \gamma_{0_A})$ remain. A second differencing of the measurements, this time be-

tween satellites, leads to further cancellation. A double-difference operator, defined as $\nabla\Delta(*)^{ji}_{AB} = \Delta(*)^{i}_{AB} - \Delta(*)^{j}_{AB}$, is used in the following double-differenced measurement equation:

$$\lambda\nabla\Delta(\phi)^{ji}_{AB} = \nabla\Delta(\rho)^{ji}_{AB} + \lambda N^{ji}_{AB} + \nabla\Delta(\nu)^{ji}_{AB} \quad (3)$$

Now the receiver clock terms have cancelled out, a key result for using CDGPS techniques to recover carrier phase differences in a non-phase-synchroized array. Additionally, the double-differenced bias term $N^{ji}_{AB} = (\gamma^{i}_{0_B} - \gamma^{j}_{0_B}) - (\gamma^{i}_{0_A} - \gamma^{j}_{0_A})$ is now guaranteed to be an integer and is referred to as the integer ambiguity. Double-differenced measurements are repeated for all commonly visible satellite pairs, and those measurements are used to resolve the integer ambiguities and to compute the relative position vector.

Equations (1) through (3) assume a quiet ionosphere. Consider the situation where the signals encounter irregularities in the ionosphere. The measured phase becomes

$$\lambda\phi^{j}_{A} = \rho^{j}_{A} + c(\delta t_A - \delta t^{j}) + \lambda(\gamma_{0_A} - \psi^{j}_{0}) + \lambda\delta\phi^{j}_{A} + I^{j}_{A} + T^{j}_{A} + \nu^{j}_{A} \quad (4)$$

where the new term $\lambda\delta\phi^{j}_{A}$ is the product of the nominal wavelength and phase disturbance due to scintillation. After double differencing, the measurements become

$$\lambda\nabla\Delta(\phi)^{ji}_{AB} = \nabla\Delta(\rho)^{ji}_{AB} + \lambda N^{ji}_{AB} + \lambda\nabla\Delta(\delta\phi)^{ji}_{AB} + \nabla\Delta(\nu)^{ji}_{AB} \quad (5)$$

Notice that the same terms that cancelled out of Eq. (1) have canceled out here, but a double-differenced phase disturbance term remains.

For the moment, consider the terms in Eq. (5) from the perspective of trying to recover information about the disturbed ionosphere. Suppose the double-differenced range and the integer ambiguities are known. What remains are the measured double-differenced phase, the double-differenced phase due to scintillation, and a noise term. Rearranging the terms in Eq. (5) with the measured term, the known terms, and the noise term on the right, the following CDGPS measurement residual can be formed:

$$\lambda\nabla\Delta(\delta\phi)^{ji}_{AB} = \lambda\nabla\Delta(\phi)^{ji}_{AB} - \nabla\Delta(\rho)^{ji}_{AB} - \lambda N^{ji}_{AB} - \nabla\Delta(\nu)^{ji}_{AB} \quad (6)$$

This measurement residual represents a combination of the single-differenced phase disturbance from satellite i and the single-differenced phase disturbance from satellite j:

$$\lambda\nabla\Delta(\delta\phi)^{ji}_{AB} = \lambda[(\delta\phi^{i}_{B} - \delta\phi^{i}_{A}) - (\delta\phi^{j}_{B} - \delta\phi^{j}_{A})] \quad (7)$$

Given only this information, it is impossible to determine whether the ionospheric irregularities that caused the phase disturbances were encountered on the path from satellite i or satellite j, or both.

Suppose, however, that one of the signals is not scintillating, as depicted in the top drawing of Fig. 5. Then that signal's contribution to the double-differenced phase disturbance may be neglected, leaving only the phase difference between the receivers caused by disturbances on the signal from satellite i:

$$\Delta(\delta\phi)^{i}_{AB} = \lambda[(\delta\phi^{i}_{B} - \delta\phi^{i}_{A}) - \cancelto{0}{(\delta\phi^{j}_{B} - \delta\phi^{j}_{A})}] \quad (8)$$

In the authors' experience with scintillation monitoring, the assumption that at least one visible signal experiences negligible scintillation is valid in nearly all situations. Considering measurement residuals from pairs of receivers throughout the scintillation imaging array, a map of the phase differences can be constructed, as shown in bottom drawing of Fig. 5. The next section considers how these data may be used in diffraction tomography.

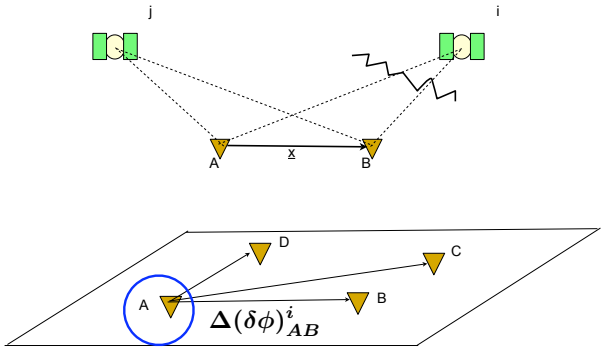

Figure 5. The relative navigation scenario with one satellite scintillating (top) and the phase relationships in the scintillation imaging array (bottom).

Before going forward, however, one question remains to be answered: How are the double-differenced range and the integer ambiguities determined? The answer is that they are the products of a calibration stage in which the relative navigation solution is computed during a quiet period prior to the onset of scintillation. Ionospheric irregularities most often occur near the magnetic equator after local sunset. Since GPS satellites are typically in view for hours, the undisturbed signals tracked before local sunset are the same signals that are disturbed at the onset of scintillation, an important and scientifically interesting stage of scintil-

lation phenomena. Since the integer ambiguities are constant, they remain valid, provided there are no cycle slips, for all continuously tracked signals—even after scintillation begins. Furthermore, the receivers in the array are static; that is, their relative position vectors are constant. If estimated, these relative position vectors may be used in conjunction with the known GPS ephemerides to calculate the double-differenced range.

PHASE DIFFERENCES IN DIFFRACTION TOMOGRAPHY

The phase differences recovered from the CDGPS measurement residuals do not contain all the information required to fully describe the phase disturbance of a GPS wavefront across a scintillation imaging array. For that, the absolute carrier phase disturbance at each receiver would have to be known. Suppose, however, that the absolute carrier phase disturbance at one receiver could be estimated. That receiver would act as an anchor for the array, allowing the absolute carrier phase disturbances at the other receivers to be computed using the measured phase differences. This concept is illustrated in the bottom drawing of Fig. 5, where receiver A acts as the array's anchor.

Two scenarios can be considered. In the first, each receiver in the array is equipped with an inexpensive frequency reference, e.g., a temperature compensated crystal oscillator. In this case, the absolute carrier phase disturbance at receiver A would have to be re-estimated at each measurement step as part of the overall tomography estimation problem. For N receivers in the array and M samples, the scintillation imaging array provides $M(N-1)$ new pieces of data to the tomography estimator.

In the second scenario, receiver A is equipped with a very stable oscillator, e.g., an ovenized crystal oscillator. For this case, consider the carrier phase measurement equation for receiver A from satellite i:

$$\lambda\phi_A^i = \rho_A^i + c(\delta t_A - \delta t^i) + \lambda(\gamma_{0_A} - \psi_0^i) + \lambda\delta\phi_A^i + I_A^i + T_A^i + \nu_A^i \quad (9)$$

Assuming that the absolute position of the receiver is known and that the bulk-quiescent ionosphere term I_A^j and troposphere term T_A^j maybe modeled and removed, the following unknowns remain: the GPS satellite ephemeris errors (the position components of which are assumed to be included in the line-of-sight range term ρ_A^i); the receiver clock error, δt_A; the real-valued carrier phase measurement biases, γ_{0_A} and ψ_0^i; and the phase disturbance due to scintillation. The combined effect of the GPS ephemeris errors, the stable receiver clock error, and the measurement biases would be nearly constant over relatively short sample periods. The tomography estimator could use data from the imaging array to estimate this bias once for a given sample period, resulting in a measurement residuals that contain the time history of the absolute carrier phase disturbances at receiver A. In this scenario, the diffraction tomography estimator gains $MN-1$ new pieces of data.

It is important to keep in mind that, until now, tomography estimators have exploited only amplitude data. The use of the phase data offered by this paper's method will improve the quality of the tomography estimates.

SOLUTION ALGORITHM

The solution algorithm is divided into four steps: calibrating the array using CDGPS techniques, detecting the onset of scintillation, identifying a non-scintillating reference signal, and recovering the phase differences between pairs of receivers.

The calibration step is carried out by performing the relative navigation solution using the CDGPS techniques described in Ref. [5]. The problem formulation in Ref. [5] employs a square-root information (SRI) implementation of a sequential least-squares estimator. The estimator assembles double-differenced carrier phase measurements for the commonly tracked pairs of satellites, considers the ambiguity *a priori* information, and performs the standard square-root information factorizations [6]. The following block upper-triangular system of equation results:

$$\begin{bmatrix} \underline{z}_{x_k} \\ \underline{z}_{N_k} \\ \underline{z}_{r_k} \end{bmatrix} = \begin{bmatrix} R_{xx_k} & R_{xN_k} \\ 0 & R_{NN_k} \\ 0 & 0 \end{bmatrix} \begin{bmatrix} \underline{x}_k \\ \underline{N} \end{bmatrix} + \begin{bmatrix} \underline{\nu}_{x_k} \\ \underline{\nu}_{N_k} \\ \underline{\nu}_{r_k} \end{bmatrix} \quad (10)$$

where the vectors $\underline{z}_{x_k}$ and $\underline{z}_{N_k}$ are the SRI vectors that associated with the relative position $\underline{x}_k$ and ambiguity $\underline{N}$ states, respectively. The matrices R_{xx_k} and R_{NN_k} are square, upper-trangular SRI matrices through which the states and the SRI vectors are related. R_{xN_k} is a dense matrix that relates the ambiguity state vector and the SRI vector $\underline{z}_{x_k}$. The terms $\underline{\nu}_{x_k}$ and $\underline{\nu}_{N_k}$ are zero-mean, unit-variance, white-noise random vectors. The vector $\underline{z}_{r_k}$ is the SRI residual, and the vector $\underline{\nu}_{r_k}$ is the associated zero-mean, unit-variance, white-noise random vector. Specialized techniques are used to resolve the integer ambiguity vector $\underline{N}$, and the relative position vector $\underline{x}_k$ is calculated by back substitution. These estimates will be used in subsequent steps to construct carrier phase difference measurement residuals.

An important feature of square-root information data processing is that, in the absence of measurement anomalies, the square-root information residual vector $\underline{z}_{r_k}$ is a Gaussian distributed, zero-mean, unit-variance random vector, i.e., $\underline{z}_{r_k} \sim \mathcal{N}(0, I)$. Measurement anomalies like carrier phase cycles slips or disturbances due to scintillation make

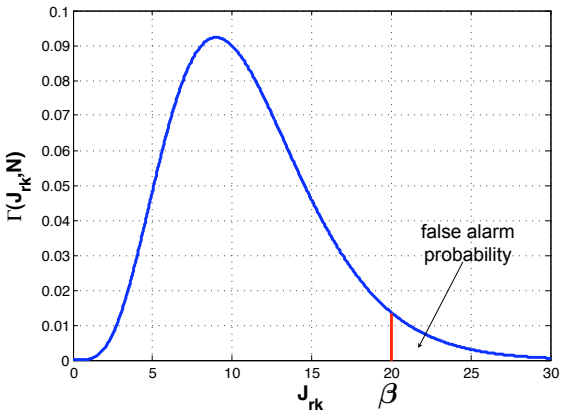

Figure 6. The Chi-squared distribution for the cost variable J_{r_k}.

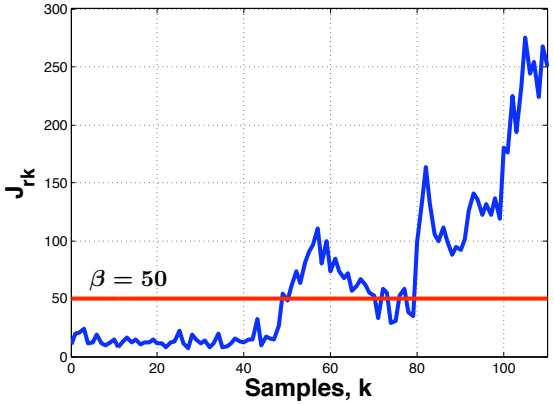

Figure 7. threshold.

$\underline{z}_{r_k}$ deviate from that distribution. This fact is used to develop a threshold test for detecting such anomalies. To this end, scalar cost is defined as the sum-of-squares of the elements of $\underline{z}_{r_k}$:

$$J_{r_k} = \sum_{p=1}^{N} (z_{r_k}^p)^2 \tag{11}$$

In this equation, the superscript p indicates the p^{th} element of the vector $\underline{z}_{r_k}$. The sum-of-squares of N Gaussian distributed random variables with zero mean and unit variance is distributed as a Chi-squared random variable with a mean of N and variance of $2N$, i.e., $J_{r_k} \sim \chi^2_N$.

For example, in the absence of cycle slips and scintillation, the cost variable J_{r_k} for $N = 11$ should be drawn from the distribution shown in Fig. 6. If an anomaly occurs, the value of J_{r_k} increases so that it appears to be drawn from the long tail of the distribution. If a value is far out on the tail, the probability that it is in fact drawn from the distribution decreases. An acceptable false alarm probability is specified as the area under the distribution's tail beyond the value of a test statistic β. (Note: the false alarm probability area in the figure is exaggerated. More realistic areas result in larger β values.) The cost at each sample is compared to the test statistic; once exceeded, the hypothesis that a measurement anomaly has occurred is accepted.

Figure 7 plots the time history of J_{r_k} computed using 50 Hz carrier phase data for another example case. Notice how the cost increases relatively slowly after the scintillation begins. This behavior differs from that of a full cycle slip in which the cost typically jumps two or more orders of magnitude. This contrast makes distinguishing between scintillation and cycle slips easy.

One may argue at this point that a more traditional approach for scintillation detection could be used, such as monitoring the commonly used S_4 index. That index however, is typically calculated by averaging data over a relatively long time interval, e.g., 30-60 s. For a real-time scintillation monitoring system, or for real-time scintillation detection in relative navigation applications, anomalies must be detected nearly instantaneously. This paper's proposed threshold test method typically achieves detection a few tenths of a second. This fast detection is illustrated in Fig. 7 in terms of 50 Hz samples.

The next step in the solution algorithm is to identify at least one non-scintillating signal. One side effect of rapidly detecting measurement anomalies is that there is insufficient information in the data history to determine which signals are free of scintillation. In order to consider more data, a second, higher threshold is set to define the endpoint of an analysis interval. In the example case, this second threshold is set to $4 \times \beta$, illustrated in Fig. 8. The interval begins at the last sample prior to the onset of scintillation for which the cost J_{r_k} is less than N, the theoretical mean for a quiet ionosphere. This interval shown between the endpoints K_1 and K_2 in Fig. 8.

The analysis of the interval data requires the formation of CDGPS measurement residuals that rely on knowledge of the relative position vectors and the integer ambiguities. Locking in these values completes the calibration step. The relative position vector is averaged over an arbitrary number of samples prior to the beginning of the analysis interval; the integer ambiguities are taken from the last estimate before the analysis interval. Once these calibration products are saved, the following double-differenced measurement residual is formed for all the possible ji-pairs of GPS satellites:

$$\nabla\Delta\phi^{ji}_{res_k} = \lambda\nabla\Delta(\phi)^{ji}_{AB} - \nabla\Delta(\rho)^{ji}_{AB} - \lambda N^{ji}_{AB} - \nabla\Delta(\nu)^{ji}_{AB} \tag{12}$$

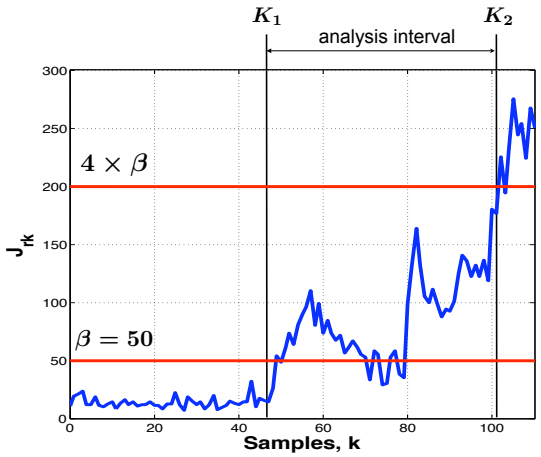

Figure 8. The analysis interval.

An interval cost is defined for each pair by summing the squares of the measurement residuals over the analysis interval:

$$J_{int}^{ji} = \sum_{k=K_1}^{K_2} (\nabla\Delta\phi_{res_k}^{ji})^2 \qquad (13)$$

Each pair is ranked according to its interval cost. Relying on the previously stated assumption that at least one signal experiences negligible scintillation, the lowest cost pair should contain at least one clean signal. The choice between the signals in the lowest cost pair is guided by considering the costs of each of those signals paired with all the remaining signals. While this selection method may be more formally posed in terms of statistical hypothesis testing, this *ad hoc* approach has proven effective.

Let the non-scintillating satellite be designated by j. Then by substituting the relative position vectors and the integer ambiguities determined from the calibration stage, the scintillation-induced phase differences between receivers A and B on the signal from satellite i can be expressed as the following CDGPS measurement residual equation, where $\lambda\nabla\Delta(\phi)_{AB}^{ji}$, $\nabla\Delta(\rho)_{AB}^{ji}$, and λN_{AB}^{ji} are known:

$$\lambda\Delta(\delta\phi)_{AB}^{i} = \lambda\nabla\Delta(\phi)_{AB}^{ji} - \nabla\Delta(\rho)_{AB}^{ji} - \lambda N_{AB}^{ji} - \nabla\Delta(\nu)_{AB}^{ji} \qquad (14)$$

RESULTS FROM TRUTH-MODEL SIMULATIONS

The solution algorithm proposed in this paper has been demonstrated in truth-model simulations. Two different simulators have been combined for this purpose. The first is a scintillation simulator that was originally developed for testing GPS receiver tracking loops. It models amplitude variations as following a Ricean distribution and the spectrum of the rapidly varying component of complex-valued scintillation as following a low-pass second-order Butterworth filter. The severity of the simulated scintillation is controlled by two parameters: the S_4 index and a decorrelation time constant τ_0. Figure 9 shows a comparison between empirically-derived scintillation data for which $S_4 = 0.91$ and $\tau_0 = 0.5$ s on the left and simulated data with the same parameters and with a nominal carrier-to-noise ratio of 45 $dB\text{-}Hz$ on the right. The top plots represent the received carrier-to-noise ratio time histories; the bottom plots represent time histories of the carrier phase disturbances due to scintillation. Notice how the deep power fades in both the empirical and simulated data are accompanied by rapid, half-cycle phase transitions. This behavior stresses a receiver's tracking loops and may cause CDGPS algorithms to diverge from the correct integer ambiguity estimates. For more details on this simulator, refer to Ref. [7].

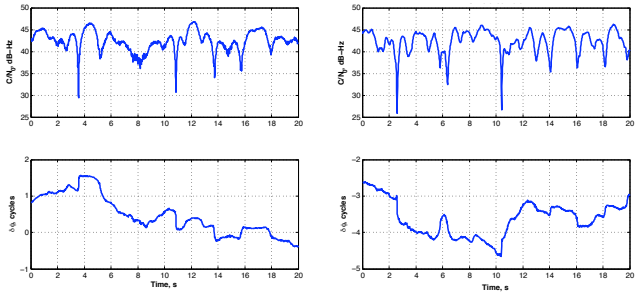

Figure 9. A comparison between empirically-derived scintillation data (left) and simulated scintillation data (right).

To generate a scintillation scenario, a typical two-receiver static baseline (100-m) CDGPS scenario is generated. A random number of GPS satellites is chosen to be scintillating. The scintillation start times are chosen randomly from a window that begins after a sufficient amount of non-scintillating data has been generated to allow the calibration stage to resolve the integer ambiguities. The S_4 and τ_0 parameters are randomly specified for both scintillating satellites and non-scintillating satellites. The scintillating satellites' parameters are drawn from a Gaussian distribution that result in strong scintillation, whereas the non-scintillating satellites' parameters are drawn from a distribution that result in weak scintillation. The mean values and standard deviations of these distributions are summarized in Table 1. Once the parameters for a particular

Table 1. Scintillation parameter distributions for simulations.

		S_4	τ_0 (s)
Strong	mean	0.9	0.5
	st. dev.	0.1	0.1
Weak	mean	0.1	30
	st. dev.	0.1	10

signal have been specified, scintillation time histories are generated at receiver *A* and receiver *B* independently. This approach does not take into account any spacial or time correlation between the scintillation received at receiver *A* and the scintillation received at receiver *B*. The authors believe this approach is reasonable considering the large separation distances envisioned. The question of correlation may be addressed in the future by using a more complicated scintillation model based on phase screens.

The carrier phase measurements are modified to include not only the scintillation-induced carrier phase disturbances but also an increase in carrier phase measurement error associated with the instantaneous drops in carrier-to-noise ratio. This phase measurement model, however, omits a potential source of error: those introduced by the phase-lock loop's inability to accurately track rapid phase changes. The question of how to design phase-lock loops that can track such phase transitions is the subject of ongoing research [8, 9]. This paper assumes that the simulated phase-lock loops exhibit robust phase tracking capability. Figure 10 shows the carrier-to-noise ratio time history for a scintillating signal at one of the receivers during a typical simulation. The scintillation begins about 12 *s* into the scenario and exhibits the typical deep fading of severe scintillation.

Before considering the results from the phase difference recovery algorithm, it is interesting to consider the effect that severe scintillation has on precise relative navigation algorithms. Figure 11 shows the relative position error magnitude time history during an example simulation. Once the integer ambiguities have been resolved, the relative position error magnitude is less than 5 *mm*. When the first deep power fade and associated phase disturbance are encountered, the relative navigation estimator diverges from the correct integer ambiguity estimates, resulting in an instantaneous jump in error from 5 *mm* to 14 *m*. The error eventually reaches 24 *m*. Errors like these may have serious consequences for certain applications—precision aircraft approach and landing, for instance.

When the phase difference recovery algorithm is applied to the simulated data, it detects the onset of scintillation in a few tenths of a second worth of data, correctly identifies a non-scintillating satellite, and provides the phase relationships between the two receivers for all of the other tracked satellites. Figure 12 shows the time history of the true and recovered phase difference between the receivers for the satellite pair that includes the reference satellite, PRN 8, and a scintillating satellite, PRN 17. Although the recovery algorithm detects the onset of scintillation quickly, it does not begin reporting phase differences until after the analysis interval. Once reporting, the recovered phase difference tracks the true phase differences well, even during the fast phase transitions that are associated with deep power fades.

Figure 13 shows a time history of the errors in the recovered phase differences. After the analysis interval,

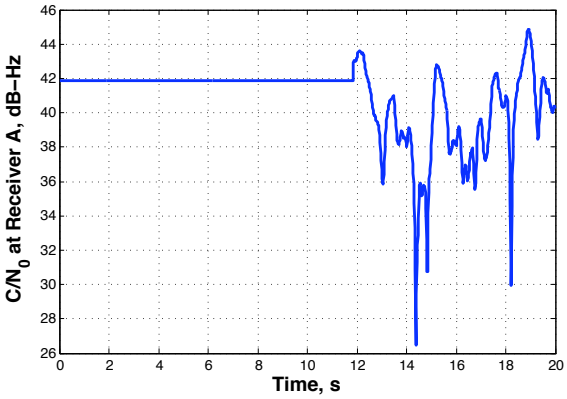

Figure 10. The time history of the received carrier-to-noise ratio at receiver *A*.

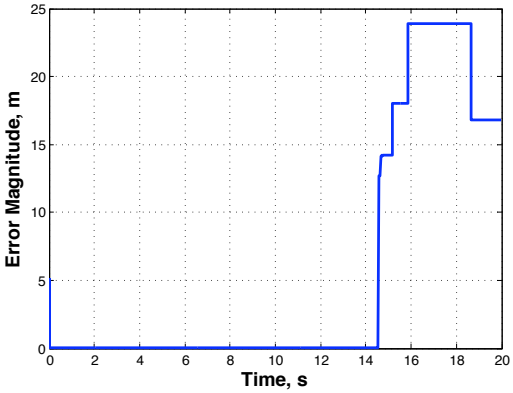

Figure 11. The time history of the relative position error magnitude during scintillation.

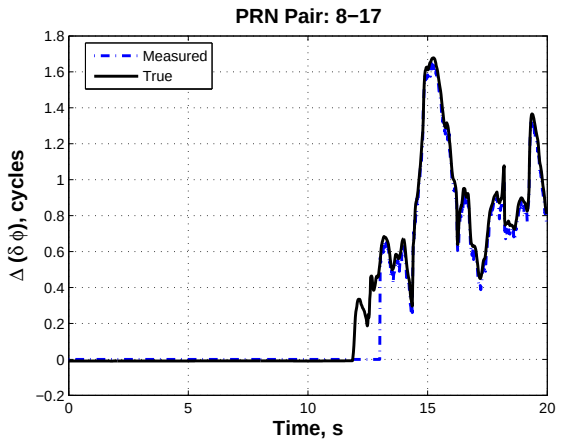

Figure 12. The time histories of the true and recovered phase differences.

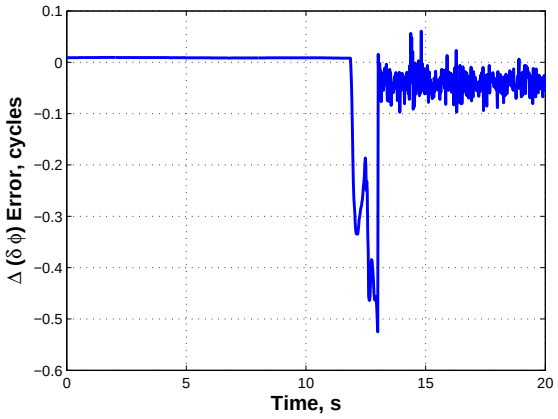

Figure 13. The time history of the error in the recovered phase differences.

which is marked by the large errors between 12 *s* and 13 *s* in scenario time, the phase difference errors are less than about 0.1 cycles and include two components: a rapidly varying part and a nearly constant part. The rapidly varying component is caused by the carrier phase measurement noise at the two receivers. Notice the jump in error when the carrier-to-noise ratio drops twice between 14 *s* and 15 *s* in scenario time. The nearly constant component is caused by the assumption that the phase disturbance due to scintillation for the reference satellite is zero. That satellite does in fact experience scintillation—very weak scintillation with a small S_4 index and a very long decorrelation time constant τ_0. The effect is a small, slowly varying phase disturbance that looks like a bias over the several seconds considered in the example scenario. Other, smaller effects that may contribute to this bias component include errors in the relative position vector estimate and errors in the broadcast GPS satellite ephemerides.

CONCLUSIONS

A method has been developed that recovers the phase relationships between pairs of independent GPS receivers operating in large scintillation imaging arrays. These phase relationships contribute to the science data that will be used to image the disturbed ionosphere with diffraction tomography techniques. The phase recovery method uses CDGPS techniques to calibrate a non-phase-synchronized array and to recover the phase differences between the receivers. The onset of scintillation is detected with a threshold test, and a method for identifying a non-scintillating reference signal has been developed. The system has been tested in truth-model simulations. The simulations generate two-receiver static baseline CDGPS scenarios that include random and systematic errors. The simulated carrier phase measurements are altered to include the effects of scintillation and the associated increase in phase measurement error.

The system rapidly detects the onset of scintillation, typically within a few tenths of a second. It defines an analysis interval, typically about 1 *s* long, that provides enough information to correctly identify a non-scintillating reference satellite. The recovered phase differences accurately represent the true phase differences, including tracking the fast half-cycle phase transitions associated with deep power fades. The errors are typically less than 0.1 cycles and have two components: a rapidly varying part that is due to the phase measurement error and a bias part that is due to the erroneous assumption that the reference signal has no scintillation effects. That signal does in fact experience very weak scintillation with a long decorrelation time constant, an effect that would appear to be a bias over the short sample periods considered in the simulations.

The diffraction tomography estimator's sensitivity to these errors has yet to be determined. If it is very sensitive, a more sophisticated, model-based approach to recovering the carrier phase disturbances may be necessary.

References

[1] Yeh, K.C., and Liu, C.-H., "Radio Wave Scintillations in the Ionosphere," *Proc. of the IEEE*, 70, 324-360, 1982.

[2] Bernhardt, P.A., Siefring, C.L., Galysh, I.J., Rodilosso, R.F., Doch, D.E., MacDonald, R.L., Wilkens, M.R., and Landis, G.P., "Ionospheric Applications of the Scintillation and Tomography Receivers in Space (CITRIS) Used with the DORIS Radio Beacon Network," *Journal of Geodesy*, Vol. 80, Nos. 8-11, Nov. 2006, pp. 473-485.

[3] Parkinson, B.W., and Enge, P.K., "Differential GPS and Integrity Monitoring," in *Global Positioning System: Theory and Applications, Vol. II*, Parkinson, B.W., and Spilker, J.J. Jr., eds., American Institute of Aeronautics and Astronautics, Washington, 1996, pp. 3-49.

[4] Psiaki, M.L., and Mohiuddin, S., "Modeling, Measurement, and Simulation of GPS Carrier-Phase for Spacecraft Relative Navigation," *Journal of Guidance, Control, and Dynamics*, to appear.

[5] Mohiuddin, S., and Psiaki, M.L., "High-Altitude Spacecraft Relative Navigation Using Carrier-Phase Differential Global Positioning System Techniques," *Journal of Guidance, Control, and Dynamics*, Vol. 30, No. 5, September-October 2007, pp. 1427-1436.

[6] Bierman, G.J., *Factorization Methods for Discrete Sequential Estimation*, Academic Press, New York, 1977.

[7] Humphreys, T.E., Psiaki, M.L, and Kintner, P.M Jr., "Simulating Ionosphere-Induced Scintillation for Testing GPS Receiver Phase Tracking Loops," to be submitted to *IEEE Transactions on Aerospace and Electrical Systems*, preprints are available upon request.

[8] Psiaki, M.L., Humphreys, T.E., Cerruti, A., Powell, S.P., and Kintner, P.M. Jr., "Tracking L1 C/A and L2C Signals through Ionospheric Scintillations," to appear in the *Proc. of the 2007 ION GNSS Conf.*, Sept. 25-28, 2007, Fort Worth, TX.

[9] Humphreys, T.E., M.L. Psiaki, B.M. Ledvina, and P.M. Kintner Jr., "GPS Carrier Tracking Loop Performance in the Presence of Ionospheric Scintillations," *Proc. of the 2005 ION GNSS Conf.*, Sept. 13-16, 2005, Institute of Navigation, Long Beach, CA.